

TEST RESULTS ON HIGH GRADIENT L-BAND SUPERCONDUCTING CAVITIES

E. Kako, S. Noguchi, M. Ono, K. Saito, T. Shishido, T. Tajima
P. Kneisel^(a), M. Matsuoka^(b), H. Miwa^(c),
T. Suzuki^(c) and H. Umezawa^(d)

KEK, National Laboratory for High Energy Physics
Oho, Tsukuba-shi, Ibaraki-ken, 305, Japan

(a) ; CEBAF, Continuous Electron Beam Accelerator Facility
12000 Jefferson Avenue, Newport News, VA 23606, USA

(b) ; MHI, Mitsubishi Heavy Industries, Ltd.
Wadasaki, Hyogo-ku, Kobe-shi, Hyogo-ken, 652, Japan

(c) ; Nomura Plating Co., Ltd.
Satsuki-cho, Kanuma-shi, Tochigi-ken, 322, Japan

(d) ; Tokyo Denkai Co., Ltd.
Higashisuna, Koto-ku, Tokyo-to, 136, Japan

Abstract

Five 1.3 GHz single-cell niobium cavities were fabricated to attain a higher accelerating gradient and to understand the phenomena limiting it. Vertical cold tests at ~ 1.8 K were carried out repeatedly on the cavities prepared by various surface treatments; *e.g.*, chemical polishing or electro-polishing, heat treatment at 760°C or 1400°C, anodization, high pressure water rinsing, etc.. A maximum accelerating gradient of 30 MV/m was achieved with no field emission after heat treatment at 1400°C. Temperature rises due to phenomena at high gradients were analyzed by 684 thermometers attached on the outer surface of the cavity.

I. INTRODUCTION

The development of high gradient superconducting cavities is essential for their application in future accelerators, such as FEL drivers, proton LINACs for neutron sources and TESLA (TeV Energy Superconducting Linear Accelerator). In the case of the TESLA application, an accelerating gradient of higher than 25 MV/m with a Q_0 value of more than 5×10^9 is required [1]. To realize this performance and so to study high gradient phenomena, a series of cavity tests has been continued at KEK since 1991. Twenty-four tests have been carried out using five 1.3 GHz single-cell niobium cavities prepared by various surface treatments. In each cavity test, maximum accelerating gradient ($E_{acc,max}$), residual surface resistance (R_{res}), limitation of $E_{acc,max}$ and heating sites were carefully investigated.

In superconducting cavities, the high gradient phenomena which limit the maximum accelerating gradient are principally multipacting, thermal breakdown and field emission. Among them, it is known that field emission is currently dominant [2,3]. The field emission phenomenon is explicated by the quantum mechanical tunneling of electrons through the modified potential barrier at the surface of a metal in a high external electric field. Dust and foreign material on the surface, chemical residue from surface treatment and surface irregularities such as projections, scratches or weld imperfections are considered to be potential sources of field emission. Therefore, smoothness and cleanness of the cavity surface are vital to the suppression of field emission phenomena. High temperature heat treatment [4,5,6], and also high pressure water rinsing [7] were found to be very effective to increase an onset field of field emission. At Cornell University, high peak power rf processing [8] was established as an *in-situ* procedure to eliminate emitters of field emission. At KEK, however, the standard procedure established for the TRISTAN superconducting cavities [9] looks good enough to attain an accelerating gradient of 30 MV/m with no field emission at least in the 1.3 GHz single-cell cavities. Instead of field emission, our serious problem is the fast breakdown and the resultant Q₀-deterioration due to field emission. This phenomenon has not been reported before, but may become a big problem at high gradients.

In this paper, we describe the cavities and the preparation methods at first, then the experimental set-up and the results of tests are reported. Finally, the phenomena at high gradients are discussed.

II. CAVITY AND PREPARATION

1. Cavities

Three kinds of cavity shapes were designed, and five single-cell cavities were fabricated; these cavities are named C-1, C-2, M-1, M-2 and K-1. All except K-1 have a spherical shape like the TRISTAN 508 MHz cavity, and K-1 has an elliptical shape scaled up from the Cornell / CEBAF 1.5 GHz cavity. The cavity shapes of these cavities are shown in Table I, together with their parameters calculated by SUPERFISH. The cavity design including the optimization of the parameters is described in reference [10]. The C-1 and C-2 cavities were fabricated at CEBAF and were made from niobium sheets of 3.2mm thick with a residual resistivity ratio (RRR) of 350. The M-1 (RRR=100) and M-2 (RRR=200) cavities were fabricated at MHI, and the K-1 (RRR=200) cavity was fabricated in the KEK machine shop. Half cells of these cavities were formed by deep drawing and were joined by electron beam welding (EBW).

2. Surface Treatment

a. Electro-polishing / Chemical polishing

The inner surface of the cavity was treated by electro-polishing (EP) or chemical polishing (CP). The amount of surface removal was measured by the decrease in the weight, and with the use of an ultrasonic thickness meter.

The electro-polishing was carried out using a horizontal rotational electro-polishing device [9], and an EP solution consisting of H₂SO₄ (95%) and HF (46%) ; (10:1 volume ratio). The current density and bath temperature were kept at around 65 mA/cm² and 35°C, respectively. The removal rate was about 0.6 μm/min.. After first electro-polishing (EP-I) or heavy EP, heat treatment for hydrogen degassing was necessary in order to prevent Q0-disease [9]. H₂O₂ (10%) rinsing for 60 min. was always carried out after the final electro-polishing (EP-II).

The CP solution was a mixture of HF (46%), HNO₃ (60%) and H₃PO₄ (85%) ; (1:1:1 volume ratio). The acid was poured into the cavity, and only the inside of the cavity was removed. Because the removal rates (ξ) in the upper and lower half-cell were different, ($\xi_{\text{upper}} = \sim 3 \times \xi_{\text{lower}}$), the cavity was inverted and the process was repeated. The removal rate was about 12 μm/min. on an average at the solution temperature of around 25°C.

Tumbling or anodization was tried in a certain test. Tumbling to polish the surface (especially, an EBW seam at an equator) was carried out using alumina tips of ~10 mm with sharp corners. The inner surface of the cavity was anodized by applying a voltage of 80 V in a solution of 10% NH₄OH, and an oxidized layer (Nb₂O₅) of ~1500 Å was formed.

b. Heat treatment

Heat treatment with titanium at 760°C was conducted to degas hydrogen dissolved in the niobium during EP-I or CP-I. The vacuum pressure at 760°C was $2 - 1 \times 10^{-5}$ Torr and the exposure time was usually 5 hours.

Heat treatment at 1400°C with titanium-gettering [11] was applied for purification. The heat treatment in the C-2 and M-1 cavities was carried out for 4 hours with the use of the CEBAF vacuum furnace. The other cavities were treated at Tokyo Denkai Co., Ltd.. In the Tokyo Denkai's vacuum furnace, the heating up time to 1400°C was 2 hours, the exposure time was 6 hours, and natural cooling was carried out for 15 hours after switching off the heater. The vacuum pressure at 1400°C was $1.0 - 0.3 \times 10^{-5}$ Torr and the dominant components of the residual gases were H₂, CO and CO₂ ; (in the ratio of 1 : 2 : 0.1) . The RRR value of niobium samples was fairly improved, and the change of RRR is seen in detail in reference [12].

After heat treatment at 760°C or 1400°C, final polishing (EP-II or CP-II) was necessary in order to remove contaminated oxide layers and deposited layers of titanium vapor.

c. Rinsing

The cavity was rinsed with demineralized (resistivity of 17.6 MΩcm), filtered (0.2 μm) and ultraviolet-sterilized ultrapure water. Shower rinsing was carried out for 10 min. (recently, in the clean room). Then finally, overflow rinsing [9] combined with ultrasonic agitation (28 kHz, 4.8 kW) in the hot bath (55°C) was performed for 120 min. A high pressure water rinsing (HPR) system with 85 kg/cm² ultrapure water [13] was developed for the active removal of dust or debris on the cavity surface and was applied in some cases. A nozzle made from tungsten carbide was initially used, but its material was changed to stainless steel by the reason mentioned later.

3. Assembling

The cavity was assembled in a clean room (class 100), and was equipped with an adjustable input coupler at the bottom and a fixed monitor coupler on the top, as shown in Fig.1. Indium sealing (ϕ1.0mm) was used for joining flanges to the cavity. After baking at 85°C for 12 hours, the vacuum pressure was generally improved to lower than 2.0 x 10⁻⁹ Torr. Subsequently, the cavity was installed in the vertical cryostat.

III. EXPERIMENTAL APPARATUS

1. Cryostat

The experimental set-up for a vertical cold test is shown in Fig. 2. The helium vessel with a diameter of 320 mm and a height of 2000 mm is surrounded with thirty layers of super-insulation and a thermal shield cooled by liquid nitrogen inside the vacuum vessel. In the initial stage of the tests, a residual magnetic field of 150 mGauss inside the helium vessel existed due to the influence of the magnetized heater components. After an improved magnetic shield made from special Permalloy, which maintains a high relative magnetic permeability ($\mu_i \sim 70000$) even at low temperature, was installed in the liquid helium bath, the residual magnetic field was reduced to less than 10 mGauss.

The rf power generated by a cw 300 W solid state amplifier is supplied to the cavity through the input coupler. The input coupler made from niobium (initially copper) can be moved remotely by a stepping motor in vacuum. With the stroke of 50 mm, coupling (Q_{in}) of the input coupler can be adjusted between 1×10^8 and 5×10^{10} to match the cavity (Q_0). Coupling (Q_{ext}) of the monitor coupler made from stainless steel is fixed to $10^{11} \sim 10^{12}$.

Vacuum leaks sometimes occurred at the ceramic of the monitor coupler which was immersed in the liquid helium bath.

The cavity is evacuated by an ion pump of 60 l/sec capacity, and the vacuum pressure usually reaches $2-5 \times 10^{-9}$ at room temperature and $5-9 \times 10^{-10}$ at low temperature. The cooling of liquid helium is carried out by three rotary pumps (total capacity 15600 l/min.), and the helium bath temperature is reduced from 4.2 K to around 1.8 K.

2. Diagnostic Systems

a. Temperature mapping

Temperature rises due to the power deposition from electron impact or enhanced losses by rf surface current can be detected by thermometers attached on the outer surface of the cavity. A temperature mapping system consisting of 684 thermometers was developed to investigate in detail the mechanism of phenomena occurring at high gradients. In order to increase the thermal sensitivity under superfluid helium, it is essential that the sensors of the thermometers possess good thermal contact to the niobium surface and efficient thermal insulation against the surrounding helium. A carbon resistor (51 Ω , Allen-Bradley) is embedded in a housing made of STYCAST for thermal insulation. The carbon of the resistor is exposed only at the contact surface with the niobium, and the contact surface of the carbon is coated with an electrical insulating thin layer. The sensor is bonded to the niobium surface using varnish with good thermal conductivity at low temperature, and is fixed firmly by springs from the support board. Nineteen sensors spaced about 10 mm apart in one meridian are attached every 10 degrees in the azimuthal direction. In Fig. 3, a schematic drawing of one meridian board consisting of 19 sensors is illustrated, and the surface electric field (E_s) and the surface magnetic field (H_s) at the location of the sensors are indicated. The surface peak electric field is located in the middle of #2 and #3 at the upper iris and in the middle of #17 and #18 at the lower iris. The surface magnetic field is almost constant in the location of #5 ~ #15. A photograph of two meridian boards made from G-10 are shown in Fig. 4. Figure 5 shows a cavity with all thermometric sensors attached. The 720 manganin lead-cables ($\phi 0.1$ mm) connected with 36 boards are taken out from the helium vessel with a special feed-through hardened by an epoxy resin. The data acquisition system is the same as that described in reference [14]. The scanning time of the whole thermometer is about 20 seconds. The temperature dependence of the resistivity of the thermometers is measured during each cooling down. The measured resistance ($R_n(T)$; n'th thermometer) of each carbon resistor is individually fitted using the following equation [15]; $\log R_n(T) + K_n / \log R_n(T) = A_n + B_n / T$, (A_n , B_n and K_n are the constants, and T is the temperature). The

temperature rise (ΔT) in the cavity test is defined as the difference from the temperature of liquid helium. The thermal sensitivity is 5 mK in this temperature mapping system.

b. X-ray monitor

Field emitted electrons are accelerated by rf electro-magnetic fields in the cavity and impact elsewhere on the cavity surface resulting in the emission of bremsstrahlung x-rays. Eight PIN photo-diodes are arrayed in one meridian outside of the thermometers. The PIN photo-diode (S1722 made by Hamamatsu Photonics Co., Ltd.) is sensitive to the x-rays in the energy range of 1 keV \sim 10 MeV [16]. A reverse biased voltage of 30 V is usually applied, and the current intensity is directly measured by a 1 M Ω terminator.

IV. EXPERIMENTAL PROCEDURE

1. Cooling down

Prior to the test, pre-cooling with liquid nitrogen is carried out in order to reduce consumption of liquid helium. The cavity is usually cooled down from room temperature to 77K in about 2 hours. Liquid nitrogen which is introduced to the bottom of the helium vessel is vaporized by 100 W heaters for one night to cool down the whole helium vessel. The cavity temperature becomes 4.2 K within 1 hour by liquid helium. In order to maintain enough helium, the transfer of liquid helium to the helium vessel is continued during pumping down, until the vapor pressure becomes about 200 Torr. The testing time available at 1.8 K is 4 hours on an average. Consumption of the liquid helium in one test is about 300 l, and that of the liquid nitrogen is about 250 l.

2. RF Measurement

The frequency of the signal generator is tuned to the resonant frequency of the cavity by a phase lock feed-back loop. The phases of input power to the cavity and the transmitted power through the cavity are compared after being down converted to 1 MHz by mixers. The error signal is fed to the DC-FM port of the signal generator in order to maintain tuning of the resonant frequency.

The input power to the cavity (P_i), reflected power from the cavity (P_r) and transmitted power through the cavity (P_t) are measured and corrected for rf losses in each cable. Cavity loss (P_0) is calculated from the balance of each power; $P_0 = P_i - P_r - P_t$. The coupling coefficient, $\beta = 1$ is suitable to improve the accuracy of the measurement; *i.e.*, matching condition, $P_r \sim 0$ as explained below. The loaded Q value (Q_L) is obtained by the decay time (τ) of the stored energy ; $P(t) = P(0) \exp\{-\omega_0 t / Q_L\}$ and $Q_L = \omega_0 \tau_{0.5} / \ln 2$.

(ω_0 is resonant frequency). The unloaded Q value (Q_0) is calculated by the following equation;

$$Q_0 = Q_L (1 + \beta_i + \beta_t).$$

Here, $\beta_t = P_t / P_0$ and $\beta_i = \beta (1 + \beta_t)$, where $\beta = \{ 1 + (P_r / P_i)^{0.5} \} / \{ 1 - (P_r / P_i)^{0.5} \}$ in over-coupling and $\beta = \{ 1 - (P_r / P_i)^{0.5} \} / \{ 1 + (P_r / P_i)^{0.5} \}$ in under-coupling. The measurements are usually carried out under the condition of $\beta = \sim 1.0$ and $\beta_t \ll 1.0$.

The accelerating gradient is given by the following equation;

$$E_{acc} = Z (P_0 * Q_0)^{0.5} .$$

Here, $Z = (R/Q)^{0.5} / l$, $l = \lambda / 2$ in a single-cell cavity, and R/Q is calculated by SUPERFISH as given in Table I. The external Q value (Q_{ext}) of the monitor coupler is calibrated by $P_0 * Q_0 = P_t * Q_{ext}$. Therefore, the accuracy of this measurement method depends mainly on P_i and $\tau_{0.5}$, and the error is estimated to be less than 10 %.

The temperature dependence of the Q_0 value at low field was measured by the above mentioned method during cooling down from 4.2 K to around 1.8 K. The temperature dependence of rf surface resistance (R_s) is calculated by $R_s(T) = G / Q_0(T)$, where G is the geometrical factor as given in Table I. The $R_s(T)$ is expressed by the addition of a temperature independent term (R_{res}) and a temperature dependent term (R_{BCS}), *i.e.*, $R_s(T) = R_{BCS}(T) + R_{res}$. The R_{res} is the residual surface resistance and depends on surface contaminants such as chemical residues and dust, trapped magnetic flux and niobium hydride due to hydrogen precipitation. The R_{BCS} is the BCS surface resistance derived from the BCS theory and is expressed by the following equation; $R_{BCS}(T) = A\omega^2/T \exp(-\Delta/kT)$, at $T < T_C/2$ and $hf \ll \Delta$. Here, A is the material constant, 2Δ is the energy gap of Cooper-pair-electrons and k is the Boltzmann's constant. The values of R_{res} , A and Δ/k are obtained by fitting the data of $R_s(T)$ to the above equations.

Increasing cw rf input power from a low initial power level, a high gradient test at around 1.8 K is carried out, and the Q_0 - E_{acc} curve is obtained by computing the above equation using the calibrated Q_{ext} and the measured P_i , P_r and P_t .

V. TEST RESULTS

Vertical cold tests at ~ 1.8 K for the five single-cell cavities prepared by various surface treatments have been conducted twenty-four times. Surface treatment and heat treatment in each test are summarized in Table II, together with the attained $E_{acc,max}$ values. The results are classified to two cases. In the first case, strong field emission is observed during the first Q_0 - E_{acc} scanning; 'field emission' case. In the second case, breakdown suddenly happens without any precursor like oscillation of P_t , heating or field emission; 'breakdown' case.

After the last breakdown at the highest gradient or during the rescanning of Q_0 - Eacc curve in a few cases, the Q_0 values start to degrade due to field emission.

1. Field Emission

In eight tests, the cavities suffered from field emission and a steep decrease in Q_0 values was observed, as seen in Fig. 6 (a). The drop in Q_0 values began between 4 and 8 MV/m, and the Q_0 values at Eacc,max degraded to less than 10^9 due to strong electron loading. The field enhancement factor (β) obtained by F-N plots of $\Delta(1/Q_0)$ was usually between 200 and 400. The causes of the field emission in our tests are considered as follows.

- 1). Electron emitters, which were produced in the previous test, were not removed in two cases. The cold test in C-2 (III) was carried out after simple warming up, and in C-1 (III) test the removed thickness was only 5 μm .
- 2). HPR was applied three times, where we used the nozzle made from tungsten carbide. The water pressure dropped from 85 to 65 kg/cm^2 during these operation, and we found that the nozzle was scraped off. This contamination is presumably one of the causes in two tests, M-1 (II) and M-2 (II).
- 3). Tumbling is another possible cause for M-2 (II), and the effect might have remained in M-2 (III). Moreover, a heavy CP (100 μm) for M-2 (III) was not well controlled, it took four times longer than usual.
- 4). In the heat treatment at 1400 $^\circ\text{C}$ for M-2 (IV), we added another titanium pipe inside the cavity. Probably, titanium layers deposited on the inner surface remained after CP of 60 μm .
- 5). Many pits were found around EBW seams at an equator and an iris in the M-1 cavity. We suspect these pits are responsible for the field emission in M-1 (I) and (II).

As mentioned above, most cases are suspected to be caused by mistakes of the surface preparation. As will be shown below, we are convinced that our surface preparation techniques are reliable and good enough to achieve an accelerating gradient of 30 MV/m without field emission. High temperature heat treatment and HPR are not necessary to suppress field emission up to the Eacc of 30 MV/m in the single-cell cavities.

2. Breakdown

The Q_0 - Eacc plots for the tests limited by breakdown are shown in Fig. 6 (b) and (c), where they are classified to two groups, the tests performed for the cavities experienced heat treatment at 1400 $^\circ\text{C}$ or not. In Fig. 6 (b), C-1 (I) and C-2 (II) are the results obtained before the installation of the improved magnetic shield, and the others are after it. The difference

between C-1 (I) [CP, no heat treatment and fast cool-down] and C-2 (II) [CP, heat treatment at 760°C] indicates the effect of the heat treatment. The decrease of the Q_0 value with the increment of E_{acc} is considerably large in no heat treatment case due to the influence of hydrogen. As a result of the improved magnetic shield, the Q_0 values of above 10^{10} at low field were obtained. The highest Q_0 value was attained in C-2 (IV) just after the heat treatment at 1400°C, as shown in Fig. 6 (c).

The distribution of the achieved $E_{acc,max}$ for the sixteen tests limited by breakdown, except the eight tests limited by field emission, is shown in Fig. 7. Obviously, the cavity performances are improved after heat treatment at 1400°C, (except M-2 (VI)). The surface treatments after heat treatment at 1400°C, that is final polishing (EP-II or CP-II) and rinsing, were the same as those after 760°C heat treatment. Therefore, the difference in the performance is considered to lie in the change of the properties of the niobium bulk material, such as growth of crystal size, extent of degassing, relaxation of residual stress, improvement of thermal conductivity, the melting of micro protrusions and so on.

Repeated surface treatment makes the thickness of niobium thin, and heat treatment softens the niobium material. Unfortunately, the C-2 cavity leaked at the iris -EBW, and the M-2 cavity collapsed by atmospheric pressure.

3. Residual Surface Resistance

Residual surface resistances (R_{res}) in a series of cavity tests are shown in Fig. 8. The Q_0 -disease due to hydrogen precipitation was observed in C-1 (I) [CP 70 μm / 7 min., no heat treatment] after pre-cooling. After warming up to room temperature and fast cooling to liquid helium temperature within 1 hour, the R_{res} was considerably reduced from 900 n Ω to 60 n Ω . Relatively large R_{res} in the initial four tests were caused by the residual magnetic field (~150 mGauss) as discussed before. After the improved magnetic shield was installed, the R_{res} were reduced to 7 ~ 34 n Ω regardless of the surface treatments (EP or CP). In two tests, however, the values of R_{res} were still large. In M-1 (II) [EP 80 μm / 2.5 hours, after heat treatment at 1400°C] and M-2 (III) [abnormal CP 100 μm / "40min.", before heat treatment at 760°C], weak Q_0 -disease may have arisen from relatively long chemical exposure time.

Figure 9 shows the change of the residual surface resistances (R_{res}) with the successive surface treatment after the heat treatment at 1400°C on the C-2 cavity. The R_{res} was reduced from 14 to 7 n Ω after the heat treatment at 1400°C. After this, the R_{res} increased gradually. This might be indicating the influence of hydrogen accumulated during the successive surface treatments. The R_{res} slightly recovered from 23 to 19 n Ω after the removal of the anodized layer as tried in (VII).

4. Temperature Mapping

Temperature mapping in the M-2 (III) test is shown in Fig. 10, where stationary local heating was observed. A similar phenomenon is also seen in reference [14]. After a few minutes in the strong field emission state (A), transition to the local heating state (B) occurred suddenly. Once the input power to the cavity was lowered a little bit and the cavity was cooled, the local heating state changed to the field emission state, again. The local heating state was very stable, and thermal breakdown was not observed in spite of a normal conducting state existing at the center of the heating spot. Thermal equilibrium between heating and cooling is considered to be kept at the heating spot.

Typical temperature rises due to strong field emission loading are shown in Fig. 11 for the M-2 (IV) test. A clear ridge line of temperature rises is observed in (A). The number of heating sites increases with successive rf processing, and the Q_0 values decrease as seen in (B). Defects produced by electron bombardment may have grown in both number and size.

Figure 12 shows temperature mapping in the M-2 (V) test, in which $E_{acc,max}$ of 29.5 MV/m was achieved with no field emission. At 23 MV/m, there is no significant heating, but at 29 MV/m the deterioration of Q_0 values looks to start and the temperature map becomes noisy. Temperature rises are not observed at the upper and lower iris with a low rf surface current. A global heating might be coming up.

Once, breakdown occurring repeatedly without the deterioration of Q_0 values was observed in the C-1 (VI) test as shown in Fig. 13. A self-pulsing at 24.5 MV/m was observed only under the over-coupling condition. In the cases where the coupling was matched, the cavity tuning loop became unlocked at the instant of breakdown at 23.6 MV/m. The Q_0 values did not deteriorate after breakdown in both cases, but the accelerating gradient could not be improved further. At the instant of breakdown, a change in vacuum and x-rays was not observed. Any obvious heating sites did not exist at $E_{acc} = 23$ MV/m just below the breakdown field, as seen in (A). Considerable temperature rises (3 ~5 K) over a wide area were observed during self-pulsing, as seen in (B). The time evolutions of a reflect signal (P_r) and a transmitted signal (P_t) at the instant of breakdown are shown in Fig.14 for the conditions of both matching and over-coupling. The energy stored in the cavity was completely dissipated with a time constant of about 1 msec. Finally, the Q_0 deterioration began at a lower gradient (around 14 MV/m) after the $E_{acc,max}$ of 24.5 MV/m was attained.

VI. BREAKDOWN AND Q_0 -DETERIORATION

In all our tests, where no field emission was observed during the initial Q_0 - E_{acc} scan, the fast breakdown and the subsequent Q_0 -deterioration due to strong field emission are

common phenomena. The understanding of the mechanism triggering this phenomenon is our urgent objective.

1. Fast Breakdown

Figure 15 shows the distribution of the breakdown gradients in each test. The features of this phenomenon are summarized as follows.

- 1). The breakdown is usually accompanied with the vacuum deterioration and the x-rays, and the stored energy is completely dissipated with a time constant of about 1 msec.
- 2). The breakdown suddenly happens without any precursor.
- 3). The breakdown occurs in the field range above 11.5 MV/m, and is very frequent between 16 ~ 20 MV/m in some cases.
- 4). Usually, the last breakdown at the $E_{acc,max}$ causes the Q_0 -deterioration, but in a certain case the Q_0 -deterioration begins at a lower gradient than the $E_{acc,max}$.
- 5). The maximum breakdown field is much improved after heat treatment at 1400°C, (see Fig. 7).
- 6). The breakdown is independent of the cavity shape, the niobium material and the surface treatment, since it occurs in every cavity test.

2. Q_0 -deterioration after breakdown

The features of the Q_0 -deterioration after breakdown are summarized as follows, and the typical Q_0 - E_{acc} curve and the temperature mapping are shown in Fig. 16.

- 1). RF processing at a high field causes a further Q_0 -deterioration, and the cavity performance is never recovered. Consequently, a final Q_0 value at 8~10 MV/m becomes less than 10^9 .
- 2). In the temperature mapping, any obvious heating sites above the sensitivity does not exist before the Q_0 -deterioration, but some remarkable temperature rises in the vicinity of the iris are observed after the Q_0 -deterioration. These heating sites change to ridge lines with increasing input rf power. The temperature rises as seen in Fig. 16 are explicitly caused by energy deposition of the impact electrons due to field emission.
- 3). Rf processing in the strong field emission region increases the number of the heating sites, and also causes the deterioration of Q_0 values at low fields. Strangely, a Q_0 value at low field tends to rise with increasing an accelerating gradient, (the temperature of liquid helium was constant). Therefore, the Q_0 values have a peak at 5 ~ 7 MV/m.
- 4). After sources of field emitted electrons were generated, the performance was not recovered by simple warming up to room temperature, C-2 (III), or by the removal of 5

μm , C-1 (III). Removal of more than 15 μm is necessary in order to recover the performance, C-1 (II).

3. Understanding of the phenomenon

As mentioned above, the breakdown occurs suddenly without a precursor, and is accompanied with the vacuum deterioration and the x-rays emission. Therefore, the phenomenon seems to be not a thermal transition (quench) but an electrical breakdown in vacuum (sparking or vacuum discharge). Stored energy in the cavity is dissipated to melt and evaporate the niobium surface during vacuum discharge. As a result, some defects causing field emission is formed. Microstructures such as protrusions, cracks, scratches, pits and grain boundaries existing at a high surface electric field may contribute to the initiation of the vacuum discharge. High temperature heat treatment might make these mild. The field limitation due to such a vacuum discharge in the cavity has not been reported before. Moreover, the mechanism of the electrical breakdown under an ultra-high vacuum consists of many complex processes, and is not completely understood even on DC breakdown of metal electrodes [17]. In order to understand the mechanism of the breakdown and solve this problem, we have started to investigate vacuum discharge on niobium samples as well as on the rf cavity, as described in the following section.

VII. DC BREAKDOWN EXPERIMENT

1. Experimentation

Experiments to study vacuum discharge of niobium electrodes at room temperature have been initiated in collaboration with Saitama University. The experimental system and the experimental procedure are described in reference [18]. A pair of niobium electrodes are set in the vacuum chamber with a vacuum pressure of 1.0×10^{-10} Torr. The gap distance between electrodes can be adjusted between 10 mm and 0.3 mm. The pulsed voltage applied to the gap has a rise time of 60 μsec , a decay time of 700 μsec and a peak value of 100 kV. The energy of several joules is dissipated at the electrodes during breakdown, and this energy is comparable to the energy stored in the cavity at a high gradient.

2. Preliminary Results

The dependence of the breakdown field strength (breakdown voltage / gap length) on the number of breakdowns was investigated initially for two pairs of niobium electrodes. One pair was only machined by a lathe, and the other was then chemical polished by 100 μm . The results are shown in Fig. 17, and are summarized in Table III, with the copper data for comparison. In the copper electrodes [18], the breakdown field strength improved gradually

with each breakdown by the conditioning, and reached 183 MV/m after 500 breakdowns. In contrast, the initial breakdown field strength in the niobium electrodes was considerably higher than that of the copper electrodes. However, the second breakdown field strength deteriorated remarkably. The breakdown field strength was not recovered even after 300 breakdowns. These experimental results seem similar to the phenomenon observed in the cavity rf test.

After breakdown measurements, a scanning electron microscope (SEM) was used to inspect the electrode surface. Figure 18 shows a SEM photograph of a niobium cathode surface after 300 breakdowns (a sample treated by chemical polishing for 10 min.). Countless craters of various sizes can be seen in the circumference of the central large molten zone.

Systematic experiments with the niobium samples treated by surface preparation similar to the cavity are expected to give a helpful suggestion to understand the mechanism of the fast breakdown and the resultant Q₀-deterioration in the cavity test.

VIII. SUMMARIES

An accelerating gradient of 30 MV/m, which exceeds the value required for TESLA, was successfully obtained with no field emission in one niobium single-cell cavity.

The results of a series of single-cell cavity tests are summarized as follows.

1. Accelerating gradients of 20~30 MV/m can be achieved with a combination of the TRISTAN standard surface preparation and the heat treatment at 1400°C.
2. Field emission is not a major problem, and neither heat treatment at 1400°C nor HPR is indispensable to suppress field emission in this field region.
3. The fast breakdown and the resultant Q₀-deterioration are a very serious problem. Many observations suggest that the fast breakdown is a vacuum discharge in the cavity.
4. The heat treatment at 1400°C looks effective to push up the breakdown gradient and the maximum accelerating gradient.

IX. ACKNOWLEDGEMENTS

The authors are indebted to Prof. Y. Kimura, Prof. K. Takata and Prof. S. Kurokawa for their continuing support and encouragement. Special thanks are given to Dr. K. Hosoyama and Mr. Y. Kojima for their cooperation in supplying liquid helium. Our thanks also go to Mr. Y. Funahashi and Mr. H. Inoue for fabricating KEK in-house cavities and to Mr. S. Yoshimoto for taking SEM photographs. The authors wish to thank Dr. S.

Kobayashi of Saitama University for the collaborating experiments of breakdown field strength by pulsed DC field.

REFERENCES

- [1] M. Tigner, "Superconducting Linear Colliders", *Proc. of the LC92 ECFA Workshop on e^+e^- Linear Colliders*, Garmisch-Partenkirchen, Germany, July, 1992, pp229-242.
- [2] W. Weingarten, "On Electrical Breakdown in Superconducting Accelerating Cavities", *IEEE Trans. on Electr. Insul.*, vol.-24 No.6 (1989), pp1005-1012.
- [3] G. Mueller *et al.*, "Field Emission Loading of Superconducting Accelerator Cavities at L- and S- band Frequencies", *IEEE Trans. on Electr. Insul.*, vol.-26 No.6 (1989), pp1013-1017.
- [4] Ph. Niedermann *et al.*, "Field Emission from Broad-area Niobium Cathodes: Effects of High Temperature Treatment", *J. of Appl. Phys.*, 59 (1986), pp892-901.
- [5] Q. S. Shu *et al.*, "A Study of the Influence of Heat Treatment on Field Emission in Superconducting RF Cavities", *Nucl. Instr. & Meth.*, A278 (1989), pp329-338.
- [6] R. Roth *et al.*, "Suppression of Field Emission in Superconducting S-Band Accelerating Structures", *Proc. of the 2nd European Particle Accelerator Conference*, Nice, France, 1990, pp1097-1099.
- [7] P. Kneisel *et al.*, "Experience with High Pressure Ultrapure Water Rinsing of Niobium Cavities", in this workshop.
- [8] J. Graber, "High Power Rf Processing Studies of 3 GHz Niobium Superconducting Accelerator Cavities", Ph.D. Dissertation, Cornell University, May, 1993.
- [9] K. Saito *et al.*, "R & D of Superconducting Cavities at KEK", *Proc. of the 4th Workshop on RF Superconductivity*, KEK, Tsukuba, Japan, August, 1989, pp635-694.
- [10] E. Kako *et al.*, "Initial Tests of L-band Niobium Superconducting Cavities for Linear Collider Application", *Proc. of the 5th Workshop on RF Superconductivity*, DESY, Hamburg, Germany, August, 1991, pp751-757.
- [11] P. Kneisel, "Use of the Titanium Solid State Gettering Process for the Improvement of the performance of Superconducting RF Cavities", *J. of Less Common Metals*, 139 (1988), pp179-188.
- [12] K. Saito *et al.*, "TESLA Activity at KEK", in this workshop.
- [13] K. Saito *et al.*, "Study of Ultra-Clean Surface for Niobium SC Cavities", in this workshop.
- [14] T. Tajima *et al.*, "Temperature Mapping System Developed at KEK for Field Emission Studies on Superconducting Cavities", *Proc. of the XVth International Conference on High Energy Accelerators*, Congress Centrum, Hamburg, Germany, July, 1992, pp751-753.

- [15] J. R. Clement and E. H. Quinell, "The Low Temperature Characteristics of Carbon-Composition Thermometers", *Rev. of Sci. Instr.*, vol.-23 (1952), pp213-216.
- [16] M. Ohara, "Development of L-band superconducting RF cavities and diagnostics", Master thesis, University of Tsukuba, February, 1993.
- [17] R. V. Latham, "High Voltage Vacuum Insulation: The Physical Basis", Academic Press London, 1981.
- [18] S. Kobayashi *et al.*, "Vacuum Breakdown Strength of Vacuum-degassed Oxygen-free Copper Electrodes", *IEEE Trans. on Electr. Insul.*, vol.-28 No.4 (1993), pp500-506.

Table I. Cavity shape and its parameters.

[calculated by SUPERFISH]

Cavity	C-1, C-2	M-1, M-2	K-1
Shape			
R/Q	102 Ω	110 Ω	101 Ω
G	274 Ω	266 Ω	269 Ω
Esp/Eacc	1.78	1.89	1.83
Hsp/Eacc	43.8 Oe/MV/m	43.2 Oe/MV/m	45.2 Oe/MV/m
RRR	350	100, 200	200
thickness	3.2 mm	2.5 mm	2.5 mm
fabricated by	CEBAF	MHI	KEK



Fig. 1. A single-cell cavity (C-1).

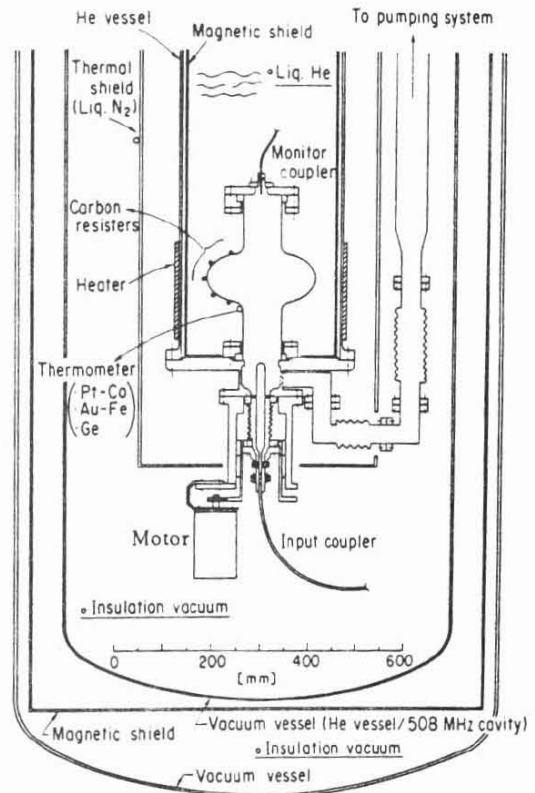


Fig. 2. Experimental set-up for a vertical cold test.

Table I. Cavity shape and its parameters.

[calculated by SUPERFISH]

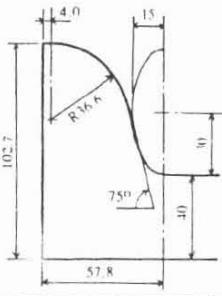
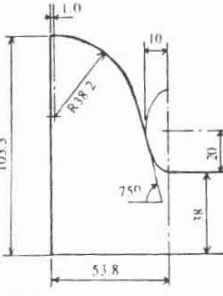
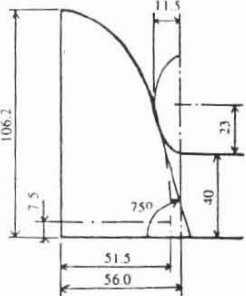
Cavity	C-1, C-2	M-1, M-2	K-1
Shape			
R/Q	102 Ω	110 Ω	101 Ω
G	274 Ω	266 Ω	269 Ω
Esp/Eacc	1.78	1.89	1.83
Hsp/Eacc	43.8 Oe/MV/m	43.2 Oe/MV/m	45.2 Oe/MV/m
RRR	350	100, 200	200
thickness	3.2 mm	2.5 mm	2.5 mm
fabricated by	CEBAF	MHI	KEK



Fig. 1. A single-cell cavity (C-1).

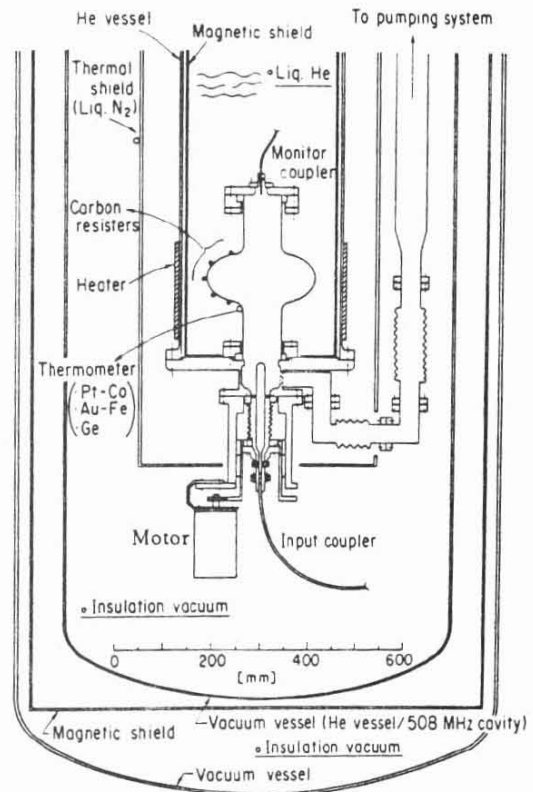


Fig. 2. Experimental set-up for a vertical cold test.

Table II. Surface preparations of 5 single-cell cavities.

Cavity	Test	RRR	Surface Treatment	Heat Treatment	Eacc,max
C-1	I	350	C.P (70 μ m)	no	14.3 MV/m
	II		C.P (10 μ m+5 μ m)	760 $^{\circ}$ C, 5 hours	15.5 MV/m
	III		HNO ₃ , C.P (5 μ m)	no	field emission
	IV		C.P (25 μ m)	no	13.6 MV/m
	V		C.P (35 μ m+50 μ m)	1400 $^{\circ}$ C, 6 hours	25.1 MV/m
	VI		C.P (50 μ m), HPR	no	24.1 MV/m
C-2	I	350	E.P (120 μ m+5 μ m)	660 $^{\circ}$ C, 24 hours	field emission
	II		C.P (30 μ m+5 μ m)	760 $^{\circ}$ C, 5 hours	15.6 MV/m
	III		no additional treatment.		field emission
	IV		E.P (100 μ m+20 μ m)	1400 $^{\circ}$ C, 4 hours	20.5 MV/m
	V		E.P (30 μ m), HPR	no	20.4 MV/m
	VI		C.P (35 μ m)	no	20.2 MV/m
	VII		C.P (30 μ m), anodization	no	17.5 MV/m
	VIII		C.P (25 μ m)	no	18.5 MV/m
	IX		<< after C.P (40 μ m), the cavity leaked at iris-EBW. >>		
M-1	I	100	E.P (110 μ m+5 μ m)	750 $^{\circ}$ C, 10 hours	field emission
	II		E.P (80 μ m), HPR	1400 $^{\circ}$ C, 4 hours	field emission
M-2	I	200	C.P (100 μ m+5 μ m)	760 $^{\circ}$ C, 5 hours	17.3 MV/m
	II		E.P (100 μ m+30 μ m) Tumbling, HPR	765 $^{\circ}$ C, 7hours	field emission
	III		C.P (100 μ m+5 μ m)	760 $^{\circ}$ C, 6hours	field emission
	IV		E.P (100 μ m)+C.P (60 μ m)	1400 $^{\circ}$ C, 6 hours	field emission
	V		E.P (115 μ m)+C.P (20 μ m)	710 $^{\circ}$ C, 8 hours	29.5 MV/m
	VI		C.P (25 μ m)	no	11.5 MV/m
	VII		<< after C.P (60 μ m), the cavity collapsed.>>		
K-1	I	200	E.P (110 μ m)+C.P(15 μ m)	710 $^{\circ}$ C, 10 hours	14.0 MV/m
	II		C.P (35 μ m+40 μ m)	1400 $^{\circ}$ C, 6 hours	17.1 MV/m

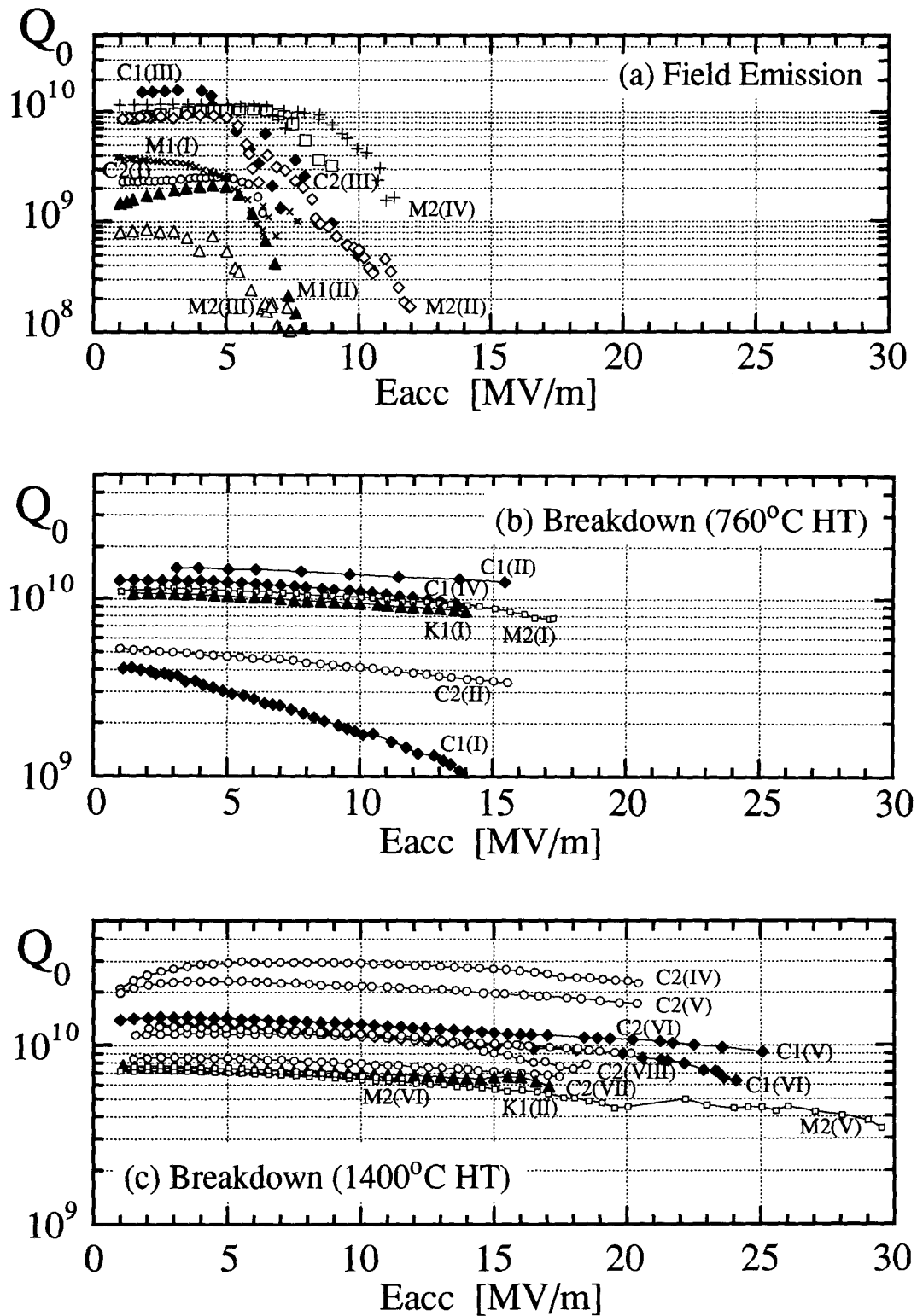


Fig. 6. Q_0 - E_{acc} plots on the cavity tests; (a) limited by field emission, (b) limited by breakdown after 760°C heat treatment, and (c) limited by breakdown after 1400°C heat treatment.

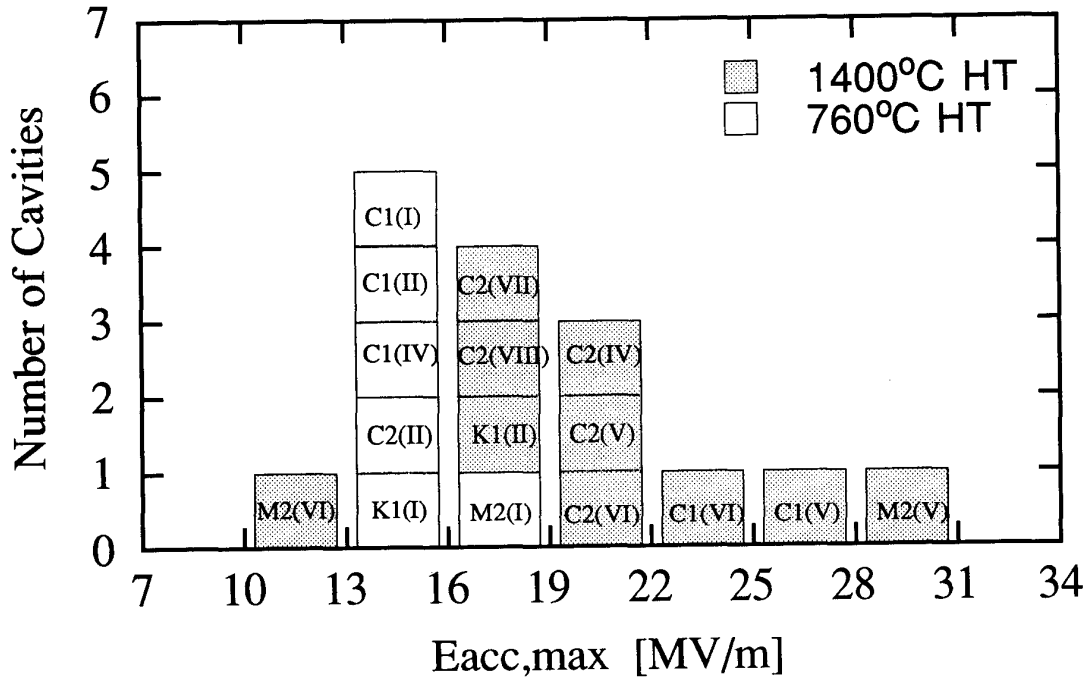


Fig. 7. Distribution of the Eacc,max for the 16 tests limited by breakdown, (except the 8 tests limited by field emission).

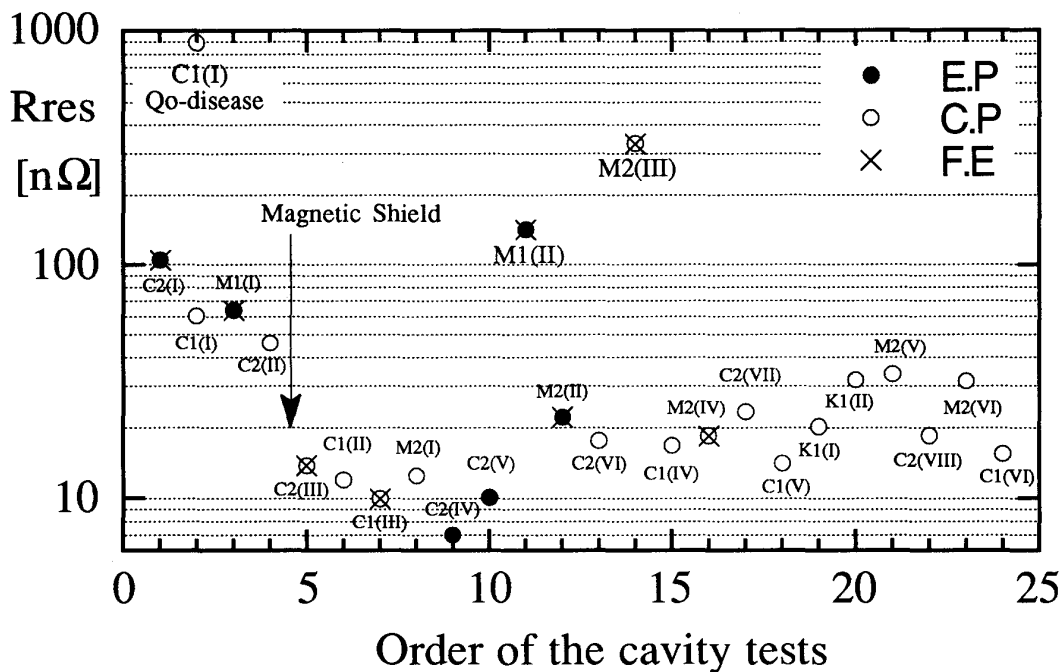


Fig. 8. Residual surface resistances (Rres) for each test, [●; electro-polished cavities, ○; chemical polished cavities, ×; limited by field emission].

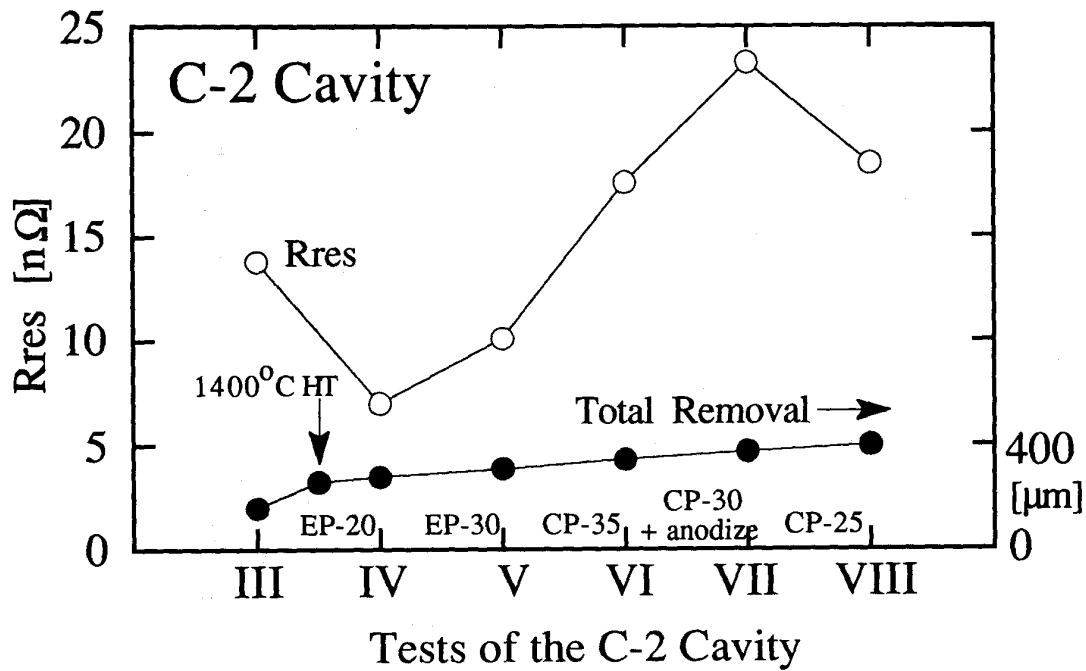


Fig. 9. Change of the residual surface resistances (Rres) with the successive surface treatment after heat treatment at 1400°C on the C-2 cavity.

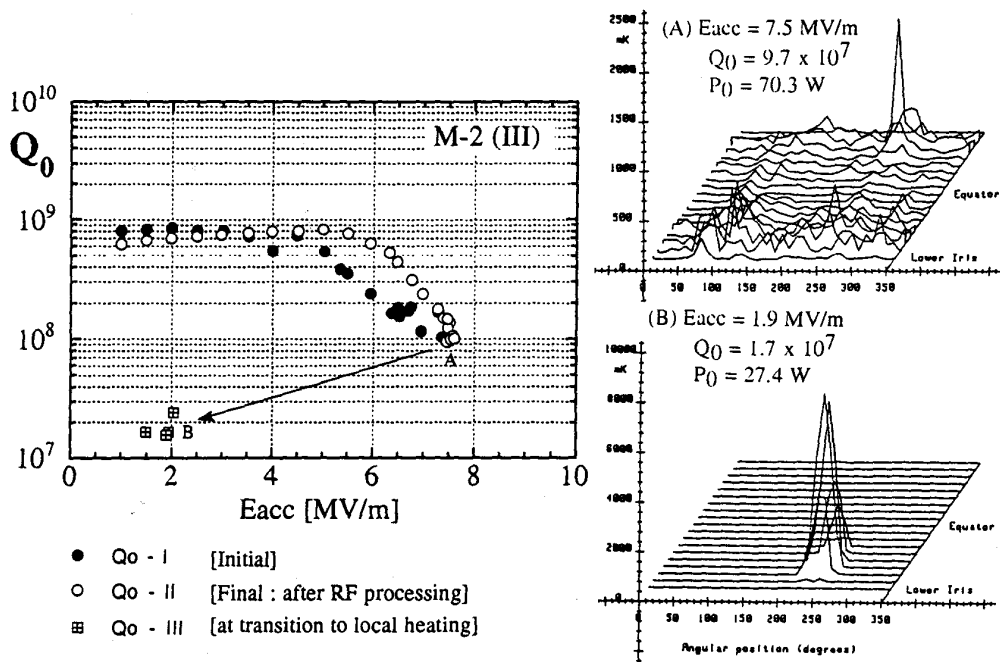


Fig. 10. Temperature rises due to stable local heating observed after transition from strong field emission region in the M-2 (III) test.

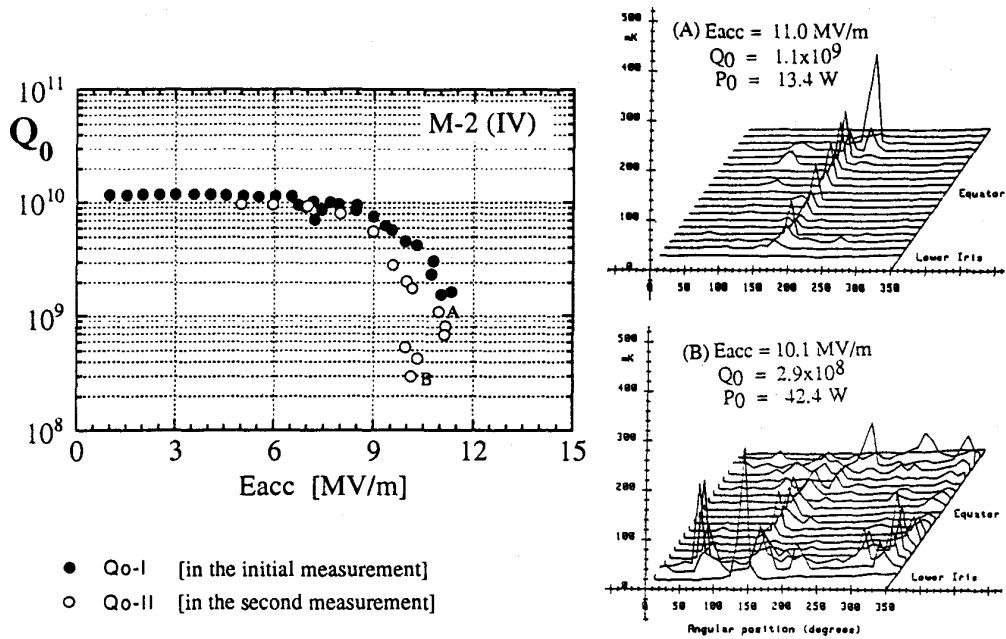


Fig. 11. Temperature rises due to strong field emission loading in the M-2 (IV) test.

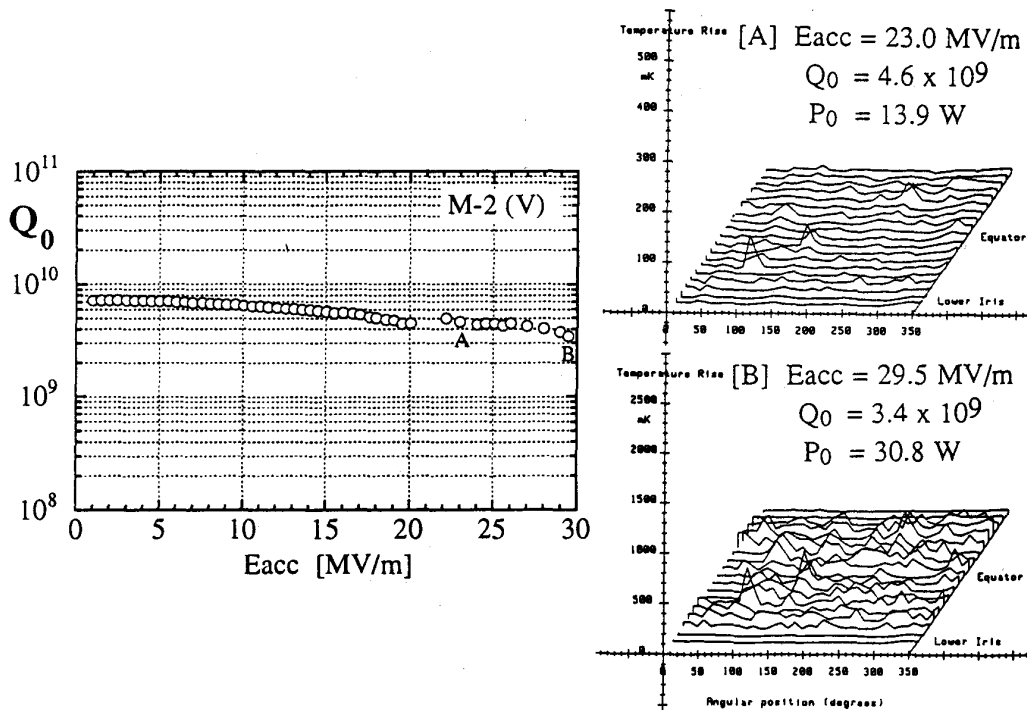


Fig. 12. Temperature rises due to losses by rf current on the cavity surface in the M-2 (V) test.

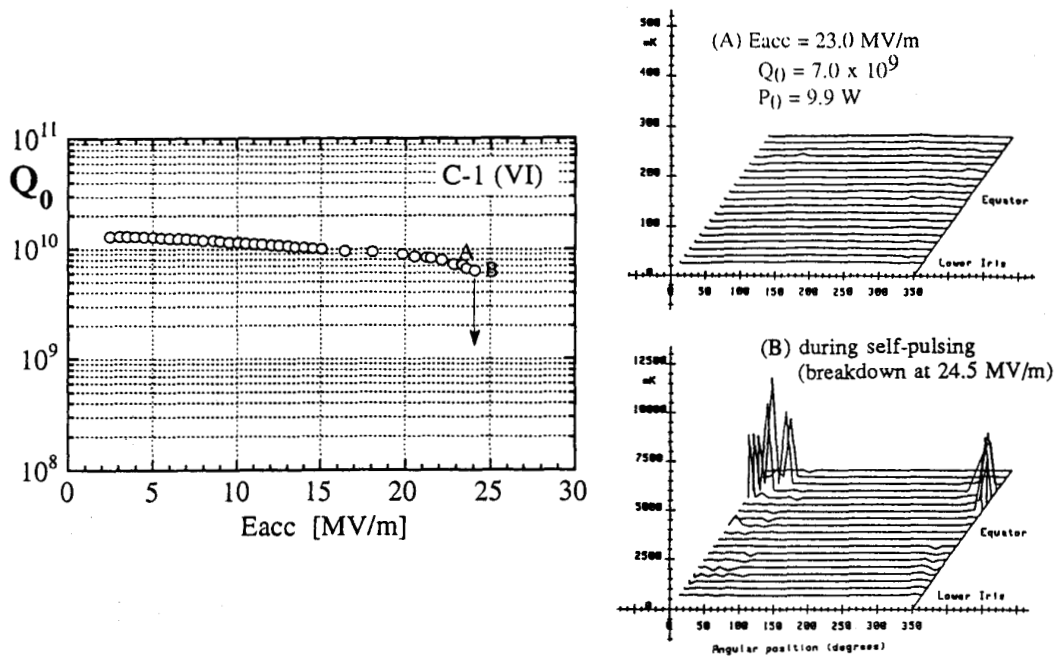


Fig. 13. Temperature rises due to breakdown occurring repeatedly (self-pulsing state) without the Q_0 -deterioration in the C-1 (VI) test.

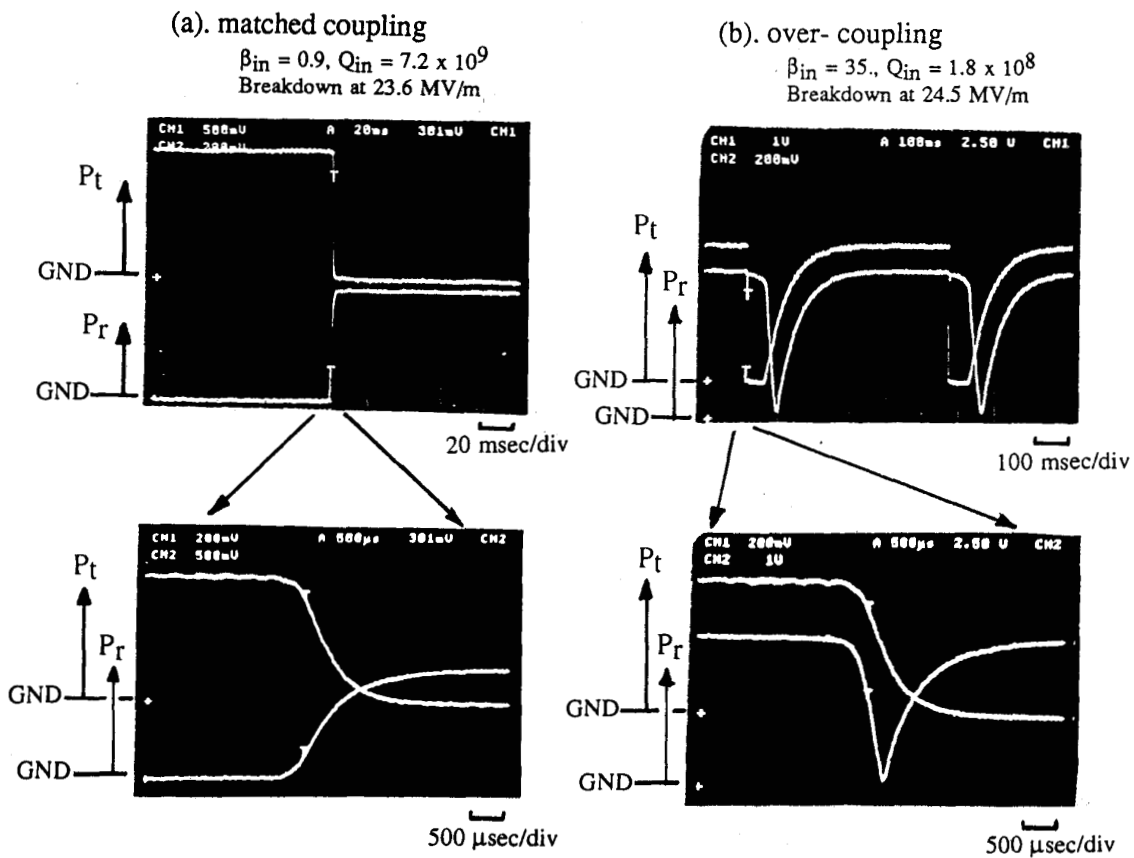


Fig. 14. Reflect signal from the cavity (P_r) and transmitted signal through the monitor coupler (P_t) at the instant of breakdown in the C-1 (VI) test, (see Fig. 10.); Coupling condition of the input coupler in (a) is matching, and that in (b) is over-coupling.

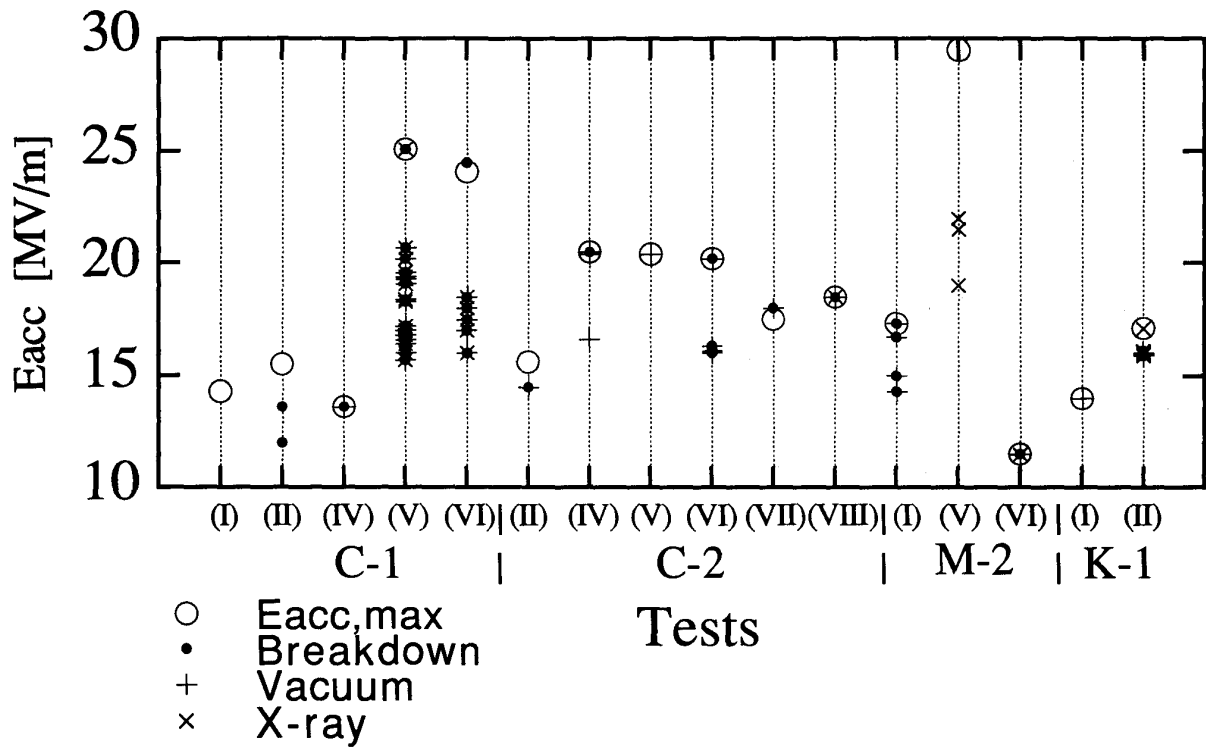


Fig. 15. Distribution of the breakdown gradients in each test.

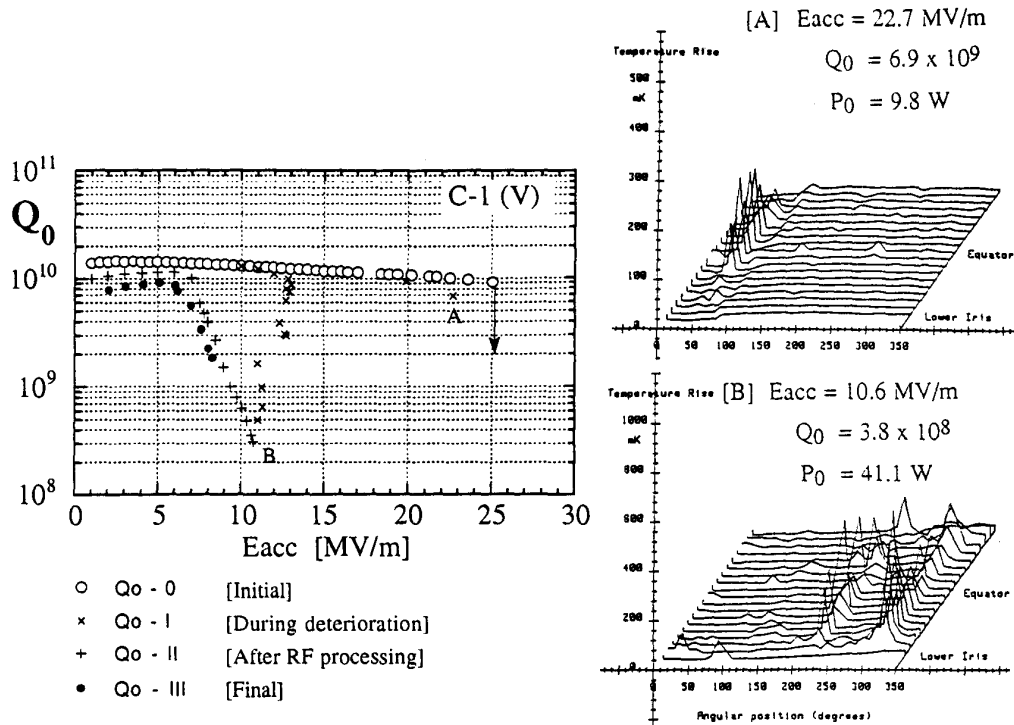


Fig. 16. Temperature rises in the Q_0 -deterioration occurring after breakdown at the Eacc,max in the C-1 (V) test.

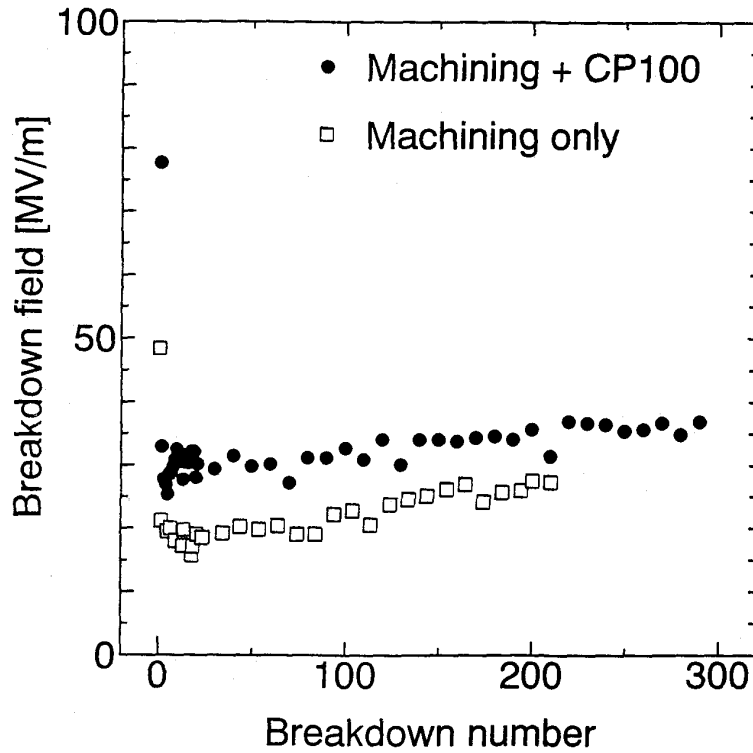


Fig. 17. Breakdown field strength on the number of breakdowns for the niobium electrodes at room temperature.

Table III. Dependence of the break-down field strength on the number of breakdowns for the niobium electrodes in comparison with that for copper electrodes. These samples were not annealed, and the electrode surfaces were pre-cleaned by *in situ* He (for Nb) or Ar (for Cu) ion beam bombardment.

Sample of electrodes	First B.D [MV/m]	Second B.D [MV/m]	100'th B.D [MV/m]	200'th B.D [MV/m]	500'th B.D [MV/m]
Nb - machining	48.	21.	23.	27.	---
Nb - CP (10 min.)	78.	33.	33.	36.	---
Cu * - machining	20.	(29.) _{10'th}	62.	98.	183.

* ; VD-OFC (vacuum degassed oxygen free copper) of class 1, from the results in ref. [18].

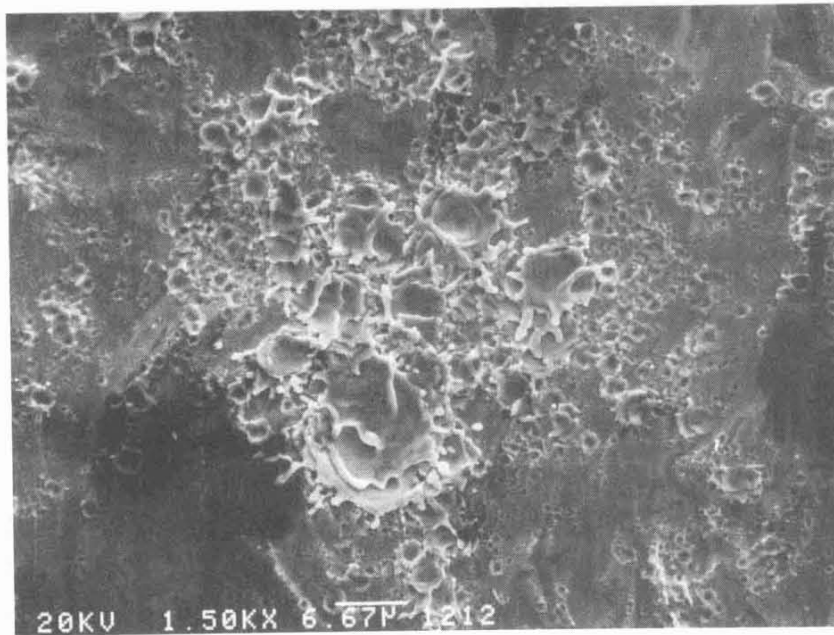


Fig. 18. A SEM photograph of a Nb (CP) cathode surface after 300 breakdowns.